BIOCHEMISTRY
including biophysical chemistry & molecular biology

Article

pubs.acs.org/biochemistry

Enzymes for the Homeland Defense: Optimizing Phosphotriesterase for the Hydrolysis of Organophosphate Nerve Agents

Ping-Chuan Tsai,[†] Nicholas Fox,[†] Andrew N. Bigley,[†] Steven P. Harvey,[‡] David P. Barondeau,*[,†] and Frank M. Raushel*[,†]

[†]Department of Chemistry, P.O. Box 30012, Texas A&M University, College Station, Texas 77842, United States

[‡]U.S. Army Edgewood Chemical Biological Center, 5183 Blackhawk Road, Aberdeen Proving Ground, Maryland 21010-5424, United States

ABSTRACT: Phosphotriesterase (PTE) from soil bacteria is known for its ability to catalyze the detoxification of organophosphate pesticides and chemical warfare agents. Most of the organophosphate chemical warfare agents are a mixture of two stereoisomers at the phosphorus center, and the S_P-enantiomers are significantly more toxic than the R_P-enantiomers. In previous investigations, PTE variants were created through the manipulation of the substrate binding pockets and these mutants were shown to have greater catalytic activities for the detoxification of the more toxic S_P-enantiomers of nerve agent analogues for GB, GD, GF, VX, and VR than the less toxic R_P-enantiomers. In this investigation, alternate strategies were employed to discover additional PTE variants with significant improvements in catalytic activities relative to that of the wild-type enzyme. Screening and selection techniques were utilized to isolate PTE variants from randomized libraries and site specific modifications. The catalytic activities of these newly identified PTE variants toward the S_P-enantiomers of chromophoric analogues of GB, GD, GF, VX, and VR have been improved up to 15000-fold relative to that of the wild-type enzyme. The X-ray crystal structures of the best PTE variants were determined. Characterization of these mutants with the authentic G-type nerve agents has confirmed the expected improvements in catalytic activity against the most toxic enantiomers of GB, GD, and GF. The values of k_{cat}/K_m for the H257Y/L303T (YT) mutant for the hydrolysis of GB, GD, and GF were determined to be 2×10^6, 5×10^5, and 8×10^5 M^{-1} s^{-1}, respectively. The YT mutant is the most proficient enzyme reported thus far for the detoxification of G-type nerve agents. These results support a combinatorial strategy of rational design and directed evolution as a powerful tool for the discovery of more efficient enzymes for the detoxification of organophosphate nerve agents.

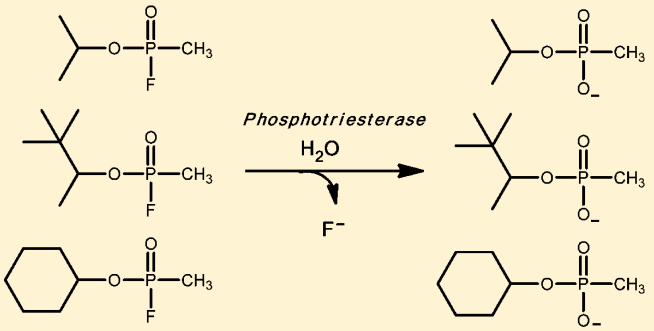

Phosphotriesterase (PTE) from *Pseudomonas diminuta* catalyzes the detoxification of a wide range of organophosphate insecticides and chemical warfare agents, including tabun (GA), sarin (GB), soman (GD), cyclosarin (GF), and VX.[1−3] The structures of these compounds are illustrated in Scheme 1. The catalytic proficiency of PTE for the hydrolysis of the insecticide paraoxon is close to the diffusion-controlled limit ($k_{cat}/K_m \sim 10^8$ M^{-1} s^{-1}),[4] and the stereoselectivity of the wild-type enzyme for chiral organophosphate substrates has been determined.[5−8] Wild-type PTE prefers to hydrolyze the R_P-enantiomers of GB, GD, GF, and their chromophoric analogues.[5,9] However, the S_P-enantiomers of these nerve agents are substantially more toxic than the R_P-enantiomers.[10] PTE mutants with an inverted stereoselectivity have been constructed by alteration of the active site residues, and these modified enzymes catalyze the hydrolysis of the toxic S_P-enantiomers faster than the wild-type enzyme.[5,11,12]

In addition to the rational redesign of the PTE active site, directed evolution of catalytic activity toward toxic organophosphates has been undertaken by several laboratories. Chen and co-workers created a randomized PTE library by DNA shuffling and saturation mutagenesis. They identified two distal mutations, K185R and I274N, which are apparently important for the improvement of the catalytic activity toward the insecticides paraoxon, parathion, chlorpyrifos, and coumaphos.[13,14] Tawfik and colleagues utilized DNA shuffling to construct randomized PTE libraries that contained variants with enhanced protein stability and increased enzymatic activity. One of these variants had three mutations located outside of the substrate binding pocket (K185R, D208G, and R319S) that increased the level of net protein expression by ~20-fold.[15] The organophosphate-degrading enzyme OpdA from *Agrobacterium radiobacter* P230 is ~90% identical to PTE. The Ollis group mutated OpdA, and libraries of these variants were created by error-prone polymerase chain reaction (PCR) and DNA shuffling. Some of these mutants were shown to have

Received: June 18, 2012
Revised: July 12, 2012
Published: July 18, 2012

   dx.doi.org/10.1021/bi300811t | *Biochemistry* 2012, 51, 6463−6475

Scheme 1

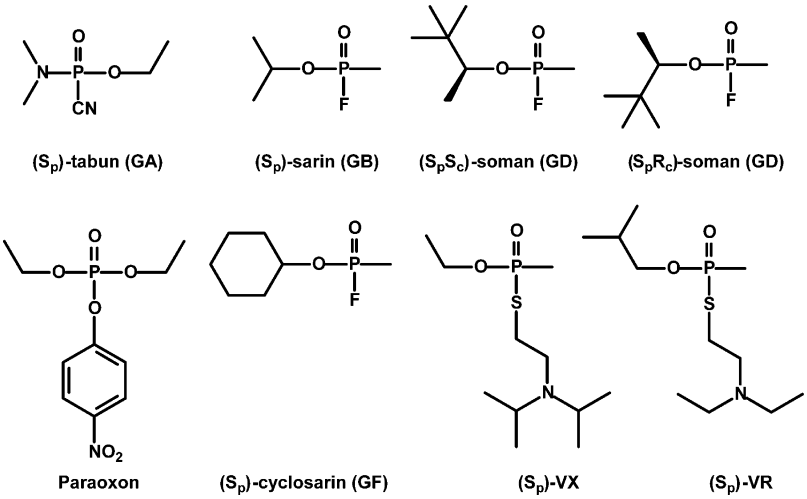

Scheme 2

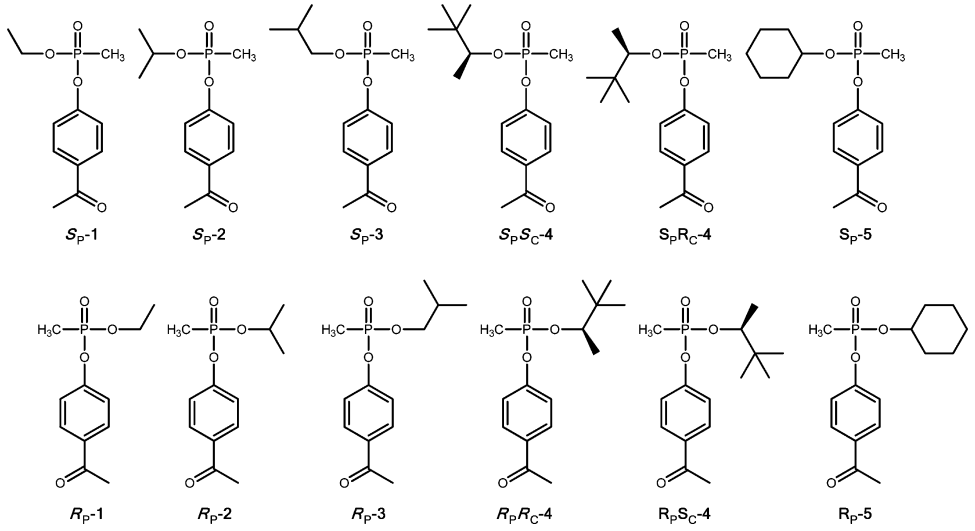

improved protein expression and better activity toward methyl paraoxon, methyl parathion, and demeton-S.[16] Many of the amino acid changes that originated from randomized mutations were localized to the surface of the protein, and these alterations may have also contributed to an increase in protein stability.[17,18]

In this paper, multiple directed evolution techniques were utilized to obtain mutant forms of PTE that are significantly enhanced in their ability to catalyze the hydrolysis of the most toxic forms of selected organophosphate nerve agents. We initiated this investigation using highly sensitive chromophoric assays to identify alterations in PTE that allow the most toxic stereoisomers of the G-agent analogues to be hydrolyzed more efficiently. An in vivo selection technique was subsequently exploited that incorporates the phosphonate assimilation pathway in *Escherichia coli* to identify beneficial PTE variants in larger, more randomized libraries. These in vivo assays utilized the coexpression of glycerophosphodiesterase (GpdQ) from *Enterobacter aerogenes* and PTE in *E. coli*. This selection method requires the enzymatic hydrolysis of phosphonate esters by PTE when these cells are grown in the absence of phosphate.[19,20] We have identified mutants of PTE with rate enhancements of more than 4 orders of magnitude relative to that of the wild-type enzyme for specific enantiomers of organophosphate nerve agent analogues. The analogue results have been validated by tests using the authentic nerve agents.

MATERIALS AND METHODS

Materials. The preparation and isolation of the chiral organophosphonates used in this investigation have been previously described.[5] The structures of these compounds are illustrated in Scheme 2. These compounds are toxic and should be used with the appropriate safeguards.

Plasmid Construction. For single-protein expression experiments, the gene for PTE was inserted between the *Nde*I and *Eco*RI restriction sites of pET20b (EMD Millipore). Plasmid GpdQ-pETDuet was constructed by inserting the gene for glycerophosphodiesterase (GpdQ) from *En. aerogenes* into the first T7 promoter site on the pETDuet (EMD Millipore) vector.[19] The PTE/GpdQ-pETDuet plasmid was created by inserting the PTE gene into the second T7 promoter site on the GpdQ-pETDuet plasmid using the *Nde*I and *Avr*II restriction sites.

Site-Directed Mutagenesis. The A80V, K185R, and I274N mutations in PTE were constructed using the QuikChange site-directed mutagenesis method from Agilent.

dx.doi.org/10.1021/bi300811t | *Biochemistry* 2012, 51, 6463−6475

Oligonucleotide pairs that contained the mutated codons at the specified sites were used as primers to amplify the genes for the wild-type enzyme and the following mutant enzymes: QF, YT, and GWT. The complete identities of mutants are listed in Table 1. The mutations were added to each template sequentially to make the following mutant proteins: RN, QFRN, YTRN, GWT-d1, and GWT-d2.

Table 1. Identification of Mutants Created for This Investigation

abbreviation	mutations
RN	K185R/I274N
QF	H254Q/H257F
GWT	H254G/H257W/L303T
QF-RN	H254Q/H257F/K185R/I274N
YT-RN	H257Y/L303T/K185R/I274N
GWT-d1	H254G/H257W/L303T/K185R/I274N
GWT-d2	H254G/H257W/L303T/K185R/I274N/A80V
GWT-d3	H254G/H257W/L303T/K185R/I274N/A80V/S61T
GWT-f1	H254G/H257W/L303T/M317L/K185R/I274N
GWT-f2	H254G/H257W/L303T/M317L
GWT-f3	H254G/H257W/L303T/M317L/I106C/F132I/L271I/K185R/I274N
GWT-f4	H254G/H257W/L303T/M317L/I106C/F132I/L271I/K185R/I274N/A80V
GWT-f5	H254G/H257W/L303T/M317L/I106C/F132I/L271I/K185R/I274N/A80V/R67H

Construction of Single- and Double-Substitution Libraries. Single-substitution (M317X) and double-substitution (W131X/F132X, S308X/Y309X, and L271X/S308X) libraries were constructed from the gene for GWT-d1 using the QuikChange (Agilent) protocol. The primers contained the degenerate codon NNS at the targeted position where N is A, T, G, or C and S is C or G. The M317X, W131X/F132X, F306X/Y309X, and S308X/Y309X libraries were created with a single set of primers. The I106X/S308X library was made using two sets of degenerate primers for the randomization of Ile-106 and Ser-308. Bacterial colonies from the unfractionated I106X library were collected, and plasmids from this library were isolated for a second round of mutagenesis using primers for the randomization of Ser-308. The double-substitution libraries, C59X/S61X and I255X/W302X, were constructed using the GWT-d2 mutant as the starting template. A single set of degenerate primers randomized the Cys-59 and Ser-61 sites. Two pairs of primers with degenerate codons for the Ile-255 and Trp-302 sites were utilized sequentially.

Construction of a Multisite Randomized Library. A multisite PTE library was constructed using the gene for GWT-f1 as the initial template. Six residues in the substrate binding pocket were partially randomized, including Ile-106, Phe-132, Leu-271, Phe-306, Ser-308, and Tyr-309. The substitutions for the Ile-106 site were alanine, cysteine, glycine, isoleucine, and valine. The variations for Phe-132 were alanine, cysteine, phenylalanine, glycine, histidine, isoleucine, leucine, proline, arginine, serine, threonine, and tyrosine. The randomized residues for the Leu-271 site consisted of phenylalanine, isoleucine, leucine, tyrosine, and glutamine. The substitution of residues for Phe-306 were phenylalanine, isoleucine, and methionine. For Ser-308, the substitutions were alanine, cysteine, glycine, serine, threonine, glutamate, leucine, glutamine, valine, and asparagine. The variants of Tyr-309 were alanine, cysteine, aspartate, phenylalanine, glycine, leucine, isoleucine, asparagine, serine, threonine, valine, tyrosine, and tryptophan.

The multisite partially randomized PTE library was constructed by combining five separate segments of the gene for PTE as illustrated in Scheme 3 using primerless PCR for 15 cycles and then amplified by PCR for 55 cycles using primers specific for the 5′- and 3′-termini. The potential size of this multisite library is 1.9×10^5 variants. In this scheme, the numbers below the residue identifier indicate the number of amino acids that were allowed during the construction of the library. The amplified PTE library was digested with *Nde*I and *Avr*II restriction enzymes and ligated into the GpdQ-pETDuet plasmid using T4 DNA ligase. The ligation mixture was purified using the QIAquick Kit (Qiagen) and then transformed into freshly made *E. coli* Top10 competent cells (Life Technologies). The transformants were incubated at 37 °C for 1 h and then plated on Luria-Bertani (LB)-ampicillin agarose. Approximately 5.7×10^5 colony-forming units (CFU) were collected and grown in LB medium for 6 h at 37 °C. The plasmids from the PTE library were extracted using the Promega Wizard Plus Miniprep kit.

Construction of the PTE Library by Error-Prone PCR. Random error-prone PCR was performed using the GeneMorph II system (Agilent). The gene for GWT-f4 served as the template, and approximately ~1.5 mutations per 1000 bp were introduced. The amplified PTE library and the GpdQ-pETDuet plasmid were digested with *Nde*I and *Avr*II and then ligated using T4 DNA ligase. The library was transformed into fresh *E. coli* Top10 competent cells (Life Technologies). The transformants were incubated at 37 °C for 1 h and then plated on LB-ampicillin agarose. Approximately 6×10^5 CFU were collected and then grown in LB medium for 6 h at 37 °C.

Growth Assays. The PTE/GpdQ-pETDuet plasmids were transformed into *E. coli* BL21(DE3) competent cells and grown on LB plates containing 0.1 mg/mL ampicillin. The colonies from fresh transformations were inoculated and grown overnight in Super Broth (32 g/L tryptone, 20 g/L yeast extract, 5 g/L NaCl, and 5 mM NaOH) at 30 °C. Overnight cultures were washed four times with sterile water to remove all

Scheme 3

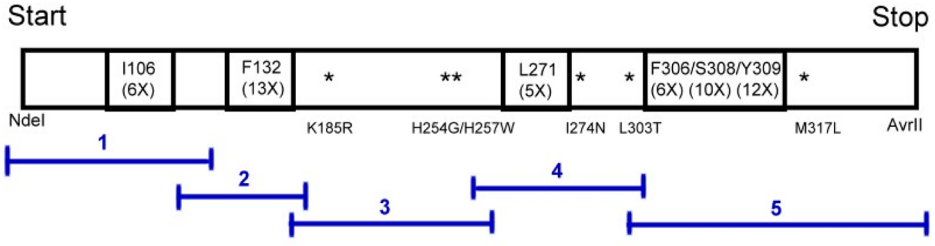

dx.doi.org/10.1021/bi300811t | *Biochemistry* 2012, 51, 6463−6475

traces of the rich medium. A 20 mL phosphate-free minimal medium (MOPS minimal medium) culture was inoculated with a 2% fresh and previously washed overnight culture as previously described.[19] The minimal medium was supplemented with 0.1% glucose as the carbon source and 0.1 mg/mL thiamine.[19] Various organophosphonate compounds were added to the cultures to a final concentration of 1.0 mM. For control experiments, BL21(DE3) cells with the empty vector (PTE-/GpdQ-) were grown in the presence and absence of inorganic phosphate. BL21(DE3) cells containing the PTE/GpdQ-pETDuet vector were induced with 0.5 mM IPTG for protein expression. Cell growth was monitored by measuring the OD_{600} for 5−10 days at 30 °C.

Screening Single- and Double-Substitution Libraries. The products of the QuikChange mutagenesis experiments were transformed into *E. coli* BL21(DE3) competent cells and inoculated in 96-deep well culture blocks containing 1.0 mL of Super Broth supplemented with 0.5 mM $CoCl_2$ and 0.1 mg/mL ampicillin. Variants of the single- and double-substitution libraries were screened with paraoxon and *p*-nitrophenol containing versions of S_P-**4**, and S_P-**5** in the presence of 2% Bug Buster. The hydrolysis of paraoxon, S_P-**4**, and S_P-**5** were measured by monitoring the formation of *p*-nitrophenol at 400 nm (ε_{400} = 17000 M^{-1} cm^{-1}) in 50 mM CHES buffer (pH 9.0) using a plate reader at 30 °C.

In Vivo Selection on Phosphate-Free Minimal Medium Plates. The PTE/GpdQ-pETDuet library was transformed into *E. coli* BL21(DE3) cells and plated on LB-ampicillin agarose. The cells were collected and grown in Super Broth at 30 °C for 12 h. The cells were washed four times with sterile water to remove any traces of the rich medium. The cells were plated on MOPS phosphate-free minimal medium agarose with 0.4 mg/mL ampicillin and 0.5 mM IPTG and grown for 7−10 days at 30 °C in the presence of 1.0 mM S_P-**5**.[19] The colonies with sizes larger than background were selected. The first round of selection used the GWT-f2 mutant as the background, and the second round used the GWT-f4 mutant as the background. Approximately 6 × 10^5 colonies from the multi-site-randomized PTE and the error-prone PTE libraries were plated for selection.

Expression, Growth, and Purification of Phosphotriesterase Mutants. The mutant phosphotriesterase plasmids were transformed into *E. coli* BL21(DE3) cells. The transformed cells were grown in LB broth overnight at 37 °C. The overnight cultures were used to inoculate 1 L of Terrific Broth (TB) containing 25 μg/mL ampicillin and 1.0 mM $CoCl_2$ at 30 °C. The expression of PTE was induced by the addition of 1.0 mM IPTG when OD_{600} reached 0.4. The cells were harvested at 4 °C by centrifugation at 6000 rpm for 10 min after the culture had been allowed to reach stationary phase after 36−42 h at 30 °C. The mutant proteins were purified according to previously reported protocols.[18]

Protein Crystallization, Data Collection, and Structure Determination. Vapor diffusion techniques were used to grow single crystals of five PTE mutants. The mutants (RN, QFRN, GWT-d2, GWT-f5, and GWT-d3) crystallized after incubation for 1 day at 22 °C. In a typical hanging drop experiment, 2 μL of the protein and 2 μL of the precipitating agent were mixed and placed on a siliconized coverslip over 500 μL of the precipitating agent. Showers of small crystals of the GWT-f3 (12 mg/mL) variant were obtained using PEG MME 5000 as a precipitant. The small crystals were crushed, serially diluted in a stabilizing solution [24% PEG MME 5000, 4% dioxane, 1.0 mM $CoCl_2$, and either 0.1 M imidazole (pH 7.0) or 0.1 M HEPES (pH 7.5)], and used as microseeds to grow crystals of the other PTE variants. Crystals of GWT-d2 (12 mg/mL), GWT-f5 (8 mg/mL), and GWT-d3 (10 mg/mL) were grown using the imidazole seeding solution. GWT-d2 crystallized in 26% PEG MME 5000; GWT-f5 crystallized in 22% PEG MME 5000 with 100 mM diethyl phosphate (**6**), and GWT-d3 crystallized in 18% PEG MME 5000. Crystals of RN (11.5 mg/mL) were generated with the HEPES seeding solution with 100 mM diethyl phosphate and 25% PEG MME 5000 as the precipitant. One large crystal of QFRN (11 mg/mL) was produced in 0.1 M MES (pH 6.0) with 18% PEG MME 5000. GWT-f5 and GWT-d3 were crystallized from the seeding solutions in the presence of 100 mM cyclohexyl methylphosphonate (**7**) using similar conditions [26% PEG MME 5000, 0.1 M imidazole (pH 7.0), and 1 mM $CoCl_2$ and 24% PEG MME 5000, 0.1 M imidazole (pH 7.0), and 1 mM $CoCl_2$, respectively]. The crystals were immersed in the well solution containing 13% ethylene glycol for 30 s and then immediately frozen in liquid nitrogen. The frozen crystals were transferred to a cassette and shipped to the Stanford Synchrotron Radiation Lightsource (SSRL) for remote data collection. Mutants RN, GWT-f5, and GWT-d3 were collected on SSRL beamline 11-1; the rest were collected on SSRL beamline 7-1. The structures of compounds **6** and **7** are presented in Scheme 4.

Scheme 4

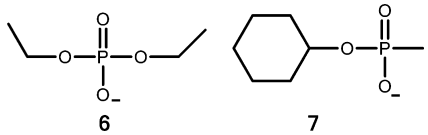

6 **7**

The data sets were indexed and scaled with the HKL2000 package,[22] and phases were determined by molecular replacement with Phaser version 2.1.[23] The search model was a previously refined PTE structure [Protein Data Bank (PDB) entry 1HZY]. Initial refinement of the structures was performed using Refmac5 from the CCP4 suite.[24,25] Difference electron density and omit maps were manually fit with the XtalView package.[26] After the cofactors (cobalt and inhibitor) were added, further refinement was conducted with CNS.[27] All structures were superimposed with Sequoia.[28] Data collection and refinement statistics are summarized in Table 2.

Kinetic Measurements and Data Analysis. The kinetic constants for each chromogenic substrate were determined by monitoring the production of *p*-acetylphenol at 294 nm (ε_{294} = 7710 M^{-1} cm^{-1}) in 50 mM CHES buffer (pH 9.0) using a plate reader at 30 °C. The protein concentration in crude samples was determined by measuring the absorbance at 280 nm. The kinetic constants (k_{cat} and k_{cat}/K_m) were obtained by fitting the data to eq 1

$$v/E_t = (k_{cat}[A])/(K_m + [A]) \quad (1)$$

where v is the initial velocity, k_{cat} is the turnover number, [A] is the substrate concentration, E_t is the enzyme concentration, and K_m is the Michaelis constant.

Kinetic constants for sarin (GB), soman (GD), and cyclosarin (GF) were determined by monitoring the release of free fluoride at 25 °C in 50 mM bis-tris-propane buffer (pH 7.2) using a fluoride electrode. Initial screenings were

Table 2. Diffraction Data Collection and Refinement Statistics[a]

	GWT-d2	QF-RN	GWT-d3	GWT-d3-(7)	GWT-f5-(6)	GWT-f5-(7)	RN-(6)
Data Collection							
beamline	BL 7-1	BL 7-1	BL 11-1	BL 7-1	BL 11-1	BL 7-1	BL 11-1
wavelength (Å)	0.9794	0.9794	0.97945	0.9794	0.97945	0.9794	0.97945
space group	$P2_12_12$	$P2_12_12$	$P2_12_12$	$P2_12_12$	$P2_12_12$	$P2_12_12$	$P2_12_12$
unit cell (Å)	85.1, 85.2, 87.7	85.6, 85.4, 88.3	85.2, 85.5, 88.1	85.5, 86.1, 88.7	85.5, 86.4, 88.1	85.5, 85.3, 87.9	85.5, 86.0, 88.0
resolution (Å)	50.0−2.00	50.0−1.95	50.0−1.89	50.0−1.95	50.0−1.77	50.0−2.1	50.0−1.60
last shell (Å)	2.07−2.00	2.02−1.95	1.95−1.89	2.02−1.95	1.83−1.77	2.18−2.10	1.66−1.60
no. of observations	418098	467416	768808	515722	1250181	303570	1586065
no. of unique observations	43780	47614	52186	48549	64191	72161	86462
redundancy	9.5 (9.2)	9.8 (8.8)	14.7 (14.5)	10.6 (10.4)	19.5 (14.1)	4.2 (4.2)	18.3 (13)
completeness (%)	99.9 (100)	99.9 (99.7)	99.9 (100)	99.7 (99.9)	99.6 (95.8)	100 (100)	100 (99.7)
mean $I/\sigma I$	23.0 (6.7)	22.8 (6.8)	23.4 (10.5)	19.1 (6.1)	44.6 (17.3)	23.3 (6.0)	38.2 (8.8)
R_{sym} (%)[b]	10.8 (38.2)	11.6 (35.5)	10.8 (32.3)	11.8 (46.1)	6.5 (19.5)	6.3 (39.5)	7.5 (31.4)
Refinement							
no. of residues in molecule A	D35−T361	D35−T361	D35−T361	D35−T361	R36−A259, N265−T361	D35−T361	D35−T361
no. of residues in molecule B	D35−I260, N265−R363	R36−I260, S267−T361	R36−I260, L262−T361	D35−T361	D35−I260, N265−T361	D35−I260, A266−T361	D35−G261, N265−T361
no. of solvent atoms	378	439	372	368	559	316	608
R_{work}/R_{free} (%)[c]	21.6/24.6	20.1/23.2	23.3/25.3	22.0/24.7	21.6/23.3	20.3/23.5	20.9/22.8
rmsd for bond lengths (Å)	0.014	0.015	0.015	0.013	0.013	0.016	0.012
rmsd for bond angles (deg)	1.67	1.61	1.66	1.63	1.63	1.63	1.59
Ramachandran plot (%)							
most favored regions	88.5	89.8	89.3	89.9	89	89.4	89.3
additional allowed regions	10.6	9.3	10	9.4	10.3	9.9	10
generously allowed regions	0.9	0.9	0.7	0.7	0.7	0.7	0.7
disallowed regions	0	0	0	0	0	0	0
PDB entry	3UR2	3UPM	3URA	3URN	3URB	3URQ	3URS

[a]Values in parentheses are the statistics for the highest-resolution shell of data. [b]$R_{sym} = \sum|I_{hkl} - \langle I\rangle|/\sum\langle I\rangle$, where $\langle I\rangle$ is the average individual measurement of I_{hkl}. [c]$R_{work} = (\sum|F_{obs} - F_{calc}|)/\sum|F_{obs}|$, where F_{obs} and F_{calc} are the observed and calculated structure factors, respectively. R_{free} is calculated the same as R_{work}, but from the data (5%) that were excluded from the refinement.

dx.doi.org/10.1021/bi300811t | *Biochemistry* 2012, 51, 6463−6475

conducted using a single fixed substrate concentration of 3.0 mM. Kinetic constants were determined for those mutants showing the highest specific activity in the initial screenings.

Stereospecificity for hydrolysis of nerve agents was obtained by following the complete hydrolysis of 0.5 mM racemic mixtures of GB or GF. Reactions were conducted in 50 mM bis-tris-propane buffer (pH 7.2) and followed by the release of fluoride. Substantial stereospecificity was observed as biphasic curves. Complementation assays were used to determine the stereopreference for variants by mixing equal units of the variant being tested with a variant with a known stereopreference. Variants with the same preference display biphasic curves when mixed, while variants of opposite preference complement each other's slow phase resulting in a single hydrolytic phase being observed. The enantiomeric preference for GB was determined by the ability of each variant to complement the hydrolysis by the YT variant. The enantiomeric preference for variants with GF was determined by the ability to complement the hydrolysis catalyzed by GWT. The enantiomeric preference of the GWT variant for GF was previously confirmed by polarimetry.[9]

RESULTS

Expression of PTE with K185R and I274N Mutations. The K185R and I274N mutations were added to the parental GWT mutant of PTE (GWT-d1). The net level of expression of soluble protein for the GWT-d1 mutant was greater than that for GWT, and approximately 10-fold more protein could be obtained following purification (data not shown). The addition of the K185R and I274N mutations to PTE variants helped to increase the levels of expression and protein yields by 2−10-fold in each case.

Screening Single- and Double-Substitution Libraries with S_P-5. The GWT mutant was previously shown to have the highest activity for the hydrolysis of the toxic S_P-enatiomers of **4** and **5**.[5] Mutant libraries were constructed using GWT-d1 as the starting template to identify more active PTE variants for the hydrolysis of S_P-**5**. Nine amino acid residues in the substrate binding pocket were considered as potential "hot spots" for the construction of these PTE libraries. The single-substitution library M317X was constructed first, followed by four double-substitution libraries (W131X/F132X, F306X/Y309X, S308X/Y309X, and I106X/Y308X). Approximately 60 colonies from the M317X library and ~550 colonies from each of the double-substitution libraries were picked and subsequently screened with S_P-**5**.

The variants with catalytic activities higher than background from the first round of screening were isolated and then rescreened with the same substrate. No improvement in the hydrolysis of S_P-**5** was found in the double-substitution libraries, W131X/F132X, F306X/Y309X, S308X/Y309X, and I106X/Y308X. Figure 1 illustrates the screening of the M317X single-substitution library. The best mutant identified in this screen contained a leucine substitution for Met-317 and is denoted GWT-f1.

Screening Double-Substitution Libraries with S_P-Enantiomers of 4. Twelve amino acid residues in the substrate binding pocket were chosen for double-substitution libraries using the GWT-d1 mutant as the starting template. The W131X/F132X, F306X/Y309X, S308X/Y309X, and I106X/Y308X libraries were screened with S_PS_C-**4** and S_PR_C-**4**, but enhanced variants were not identified. The A80V mutation was added to GWT-d1 to improve the net protein expression of PTE.[13] This mutant was denoted as GWT-d2 and shown to have better protein expression levels and a higher specific activity toward the hydrolysis of S_PS_C-**4** and S_PR_C-**4** than the GWT-d1 parent.

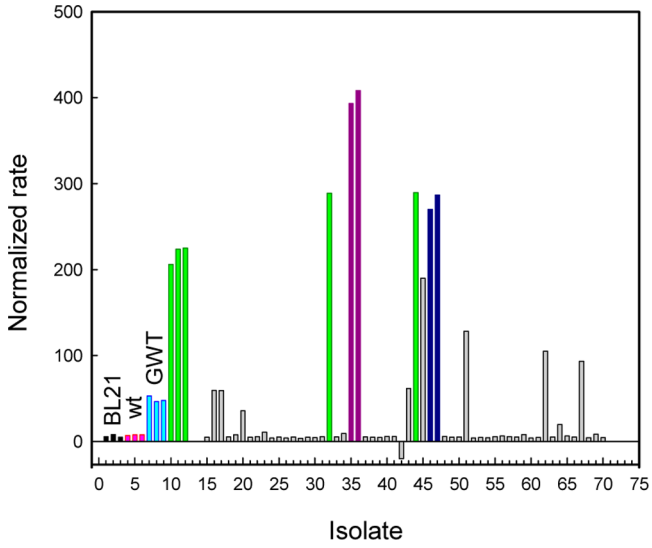

Figure 1. Screening of the M317X mutant library against S_P-**5** using GWT-d1 as the parental template. The light green, purple, and dark blue bars represent the relative catalytic activities of the GWT-d1, GWT-f1, and GWT-d1-M317F mutants, respectively. Those mutants represented by the gray bars were not characterized or sequenced.

Double-substitution libraries that randomize the residues close to the substrate binding pocket were constructed. The I255X/W302X and C59X/S61X libraries were constructed using the GWT-d2 mutant as the template. For each double-substitution library, approximately 600 colonies were selected and screened with the two S_P-enantiomers of **4**. From this screen, a mutant was identified that had more activity for the hydrolysis of S_PS_C-**4** and S_PR_C-**4**. This mutant, designated GWT-d3, contained a threonine substitution for Ser-61.

Coexpression of Phosphotriesterase and Phosphodiesterase. Mutant PTE libraries were coexpressed with a phosphodiesterase capable of hydrolyzing the reaction product to methylphosphonate,[19] and this compound is capable of supporting bacterial growth in a phosphate-free medium (Scheme 5).[29,30] The GWT-f1 mutant was partially randomized at six sites simultaneously. The total library contained 1.9×10^5 potential variants. Eight colonies from this library were selected to verify that the targeted sites were randomized (data not shown). The PTE/GpdQ-pETDuet plasmid library was transformed into *E. coli* BL21(DE3) cells. Approximately 5.8×10^5 CFU were plated on phosphate-free minimal medium with 1 mM S_P-**5** as the sole phosphorus source. The colonies that contained beneficial mutations for the hydrolysis of S_P-**5** were identified as being larger in size than a background colony of the parent GWT-f1 mutant. Approximately 30 of these colonies were selected for growth in 96-well blocks and subsequently assayed for catalytic activity with S_P-**5**. The screening of the partially randomized multisite library with S_P-**5** is shown in Figure 2a. The first nine samples include the empty vector control, wild-type PTE, and the GWT-f1 parent. A single variant was found to have more activity than the GWT-f1 parent. This mutant (GWT-f3) contained three additional changes in the amino acid sequence: I106C, F132I, and L271I.

dx.doi.org/10.1021/bi300811t | *Biochemistry* 2012, 51, 6463−6475

Scheme 5

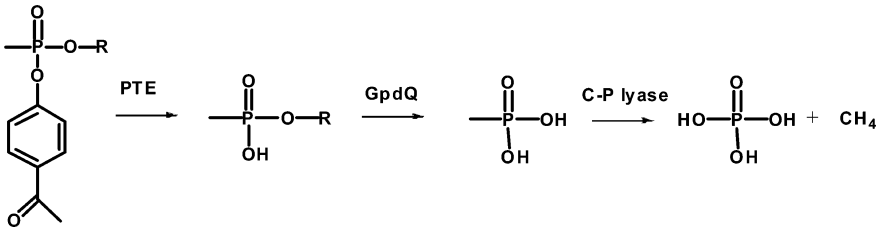

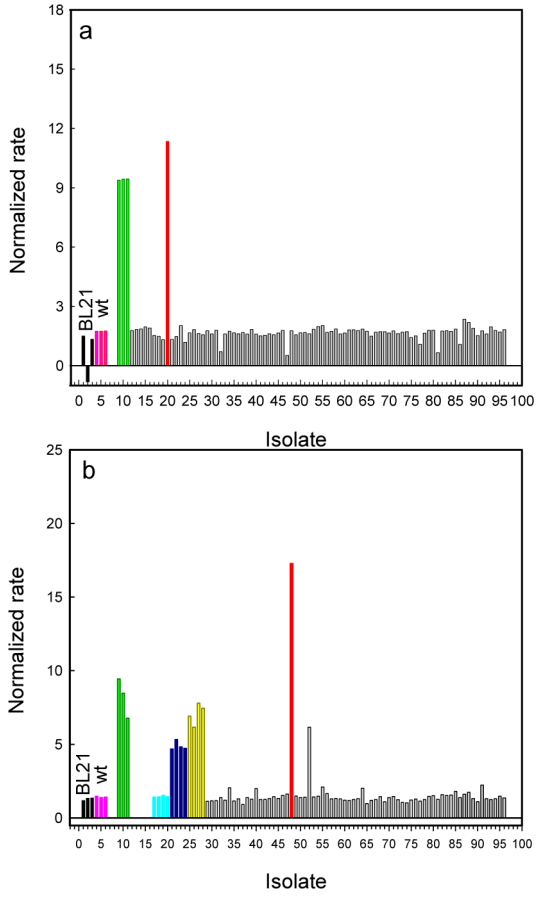

Figure 2. (a) Screening of the six-site randomized library using GWT-f1 as the parental template with S_P-**5**. The light green and red bars represent the relative catalytic activities of the GWT-f1 and GWT-f3 mutants, respectively. (b) Screening of the error-prone PCR library using GWT-f4 as the parental template with S_P-**5**. The light green, cyan, dark blue, yellow, and red bars represent the relative catalytic activities of the GWT-f4, GWT-f4-G129D, GWT-f4-I228F, GWT-f4-G254W, and GWT-f5 mutants, respectively.

The A80V mutation was added to the GWT-f3 mutant to create the GWT-f4 variant.

The GWT-f4 mutant served as the template for error-prone PCR (epPCR). Random mutagenesis of the GWT-f4 gene was conducted using the Mutazyme II DNA polymerase. Ten colonies from this library were selected to establish an average mutation rate of ~1.5 mutations/1000 bp. The epPCR-generated PTE/GpdQ-pETDuet library was transformed into *E. coli* BL21(DE3). Approximately 6×10^5 CFU were plated on phosphate-free minimal medium plates with 1 mM S_P-**5** as the sole phosphorus source. Colonies larger in size than the parental strain (GWT-f4) were assayed with S_P-**5**, and the results are shown in Figure 2b. The first 20 samples include the empty vector, wild-type PTE, GWT-f3, GWT-f3-G129D, GWT-f3-I288F, and GWT-f3-H254W. The new variant, GWT-f5, contained a single mutation, relative to GWT-f4, at Arg-67 with a change to histidine.

Kinetic Properties of the PTE Mutants. The kinetic parameters of the purified wild-type PTE and its mutants with the entire set of chiral organophosphonate compounds shown in Scheme 2 are provided in Tables 3 and 4. The best mutant (based on the value of k_{cat}/K_m) for the hydrolysis of S_P-**1** is QFRN (k_{cat}/K_m = 8.0 × 10^6 M^{-1} s^{-1}). This is also the best mutant for the hydrolysis of S_P-**2** (k_{cat}/K_m = 1.6 × 10^6 M^{-1} s^{-1}). For the hydrolysis of S_P-**3**, the best mutant identified to date is GWT-f4 (k_{cat}/K_m = 2.3 × 10^6 M^{-1} s^{-1}). For the two soman analogues (S_PS_C-**4** and S_PR_C-**4**), the best mutant is GWT-d3 (k_{cat}/K_m = 8.7 × 10^4 and 1.1 × 10^4 M^{-1} s^{-1}, respectively). GWT-f5 is the best mutant for the hydrolysis of the cyclosarin analogue, S_P-**5** (k_{cat}/K_m = 3.2 × 10^5 M^{-1} s^{-1}). The outline for the discovery of PTE variants with enhanced activity for the hydrolysis of the S_P-enantiomers of compounds **4** and **5** by directed evolution is shown in Figure 3.

Structural Analysis of Enhanced Mutants. The three-dimensional structures of RN, QF-RN, GWT-d2, GWT-d3, and GWT-f5 were determined. The backbone conformations of the residues in these proteins are quite similar to one another. Superposition of QF-RN, GWT-d3, and GWT-f5 with wild-type PTE (PDB entry 1HZY) provides Cα atom rmsd values of 0.37, 0.38, and 0.71 Å, respectively. The locations of the mutations within QF-RN, GWT-d3, and GWT-f5 are highlighted in Figure 4. The K185R and I274N mutations are on the surface of the protein. Arg-185 extends outward from α-helix 4, and Asn-274 is positioned in loop 7. The arginine in the K185R mutation forms hydrogen bond interactions with Ser-218 and Glu-219 (Figure 5A). In GWT-d3, the distance between N^{ω} of Arg-185 and the nearest carboxylate oxygen of Glu-219 is 2.8 Å, whereas the distance to the hydroxyl group of Ser-218 is 3.0 Å. The I274N mutation changes a hydrophobic residue for a hydrophilic group. In GWT-d3, the carboxamide group of Asn-274 forms a hydrogen bond interaction with the main chain amide group of itself and an additional hydrogen bond with the side chain carboxylate of Glu-263 (Figure 5B). The mutation of Ala-80 to valine does not alter the orientation of the side chain or backbone. However, the side chain of the neighboring Lys-77 within GWT-f5 and GWT-d3 is displaced up to 5.3 Å relative to the parental GWT structure (PDB entries 1P6B and 1P6C, respectively). This movement facilitates a hydrogen bond interaction between Lys-77 and Glu-81 (Figure 5C). The R67H mutation in GWT-f5 is positioned at the interface of two subunits. In the parental structure, the arginines from different subunits appear to form a hydrogen bond interaction with each other (3.1 Å). In the structure of GWT-f5, there is an imidazole from solvent that is

dx.doi.org/10.1021/bi300811t | *Biochemistry* 2012, 51, 6463−6475

Table 3. Values of k_{cat} (s^{-1}) for Wild-Type PTE and Its Mutants[a]

	WT	QF	YT	RN	QFRN	YTRN	GWT	GWT-d1	GWT-d2	GWT-d3	GWT-f1	GWT-f2	GWT-f3	GWT-f4	GWT-f5
R_P-**1**	1.5e2	1.7e2	7.3e0	9.0e1	2.0e2	1.2e1	1.4e1	1.4e1	1.3e1	9.6e0	1.3e1	2.2e2	7.9e1	ND	ND
S_P-**1**	6.7e2	3.2e1	4.1e2	8.2e2	4.5e1	1.0e3	1.9e2	2.9e2	5.3e2	4.0e2	3.6e2	4.4e2	6.6e2	1.1e3	7.2e2
R_P-**2**	1.0e2	4.8e1	1.8e1	6.6e1	6.6e1	2.0e1	ND	2.1e1	2.2e1	5.9e1	9.8e0	3.3e1	ND	ND	ND
S_P-**2**	4.0e1	7.2e0	3.7e2	2.0e1	1.1e1	7.0e2	9.2e1	8.6e1	1.3e2	2.0e2	3.0e2	2.3e2	6.2e2	1.1e3	5.9e2
R_P-**3**	9.3e1	7.0e1	5.1e1	4.8e1	1.3e2	4.3e1	2.0e1	8.0e0	1.3e1	2.2e1	2.9e1	3.4e1	1.3e1	1.5e1	ND
S_P-**3**	2.2e1	6.3e0	1.0e2	1.6e1	1.3e1	7.7e2	5.0e1	5.5e1	5.8e1	6.0e1	8.0e1	8.8e1	1.4e2	2.5e2	1.8e2
R_PR_C-**4**	3.4e0	5.5e−1	4.1e−1	4.5e0	1.1e0	5.8e−1	2.0e0	2.4e0	4.3e0	ND	4.0e0	ND	ND	ND	2.9e0
R_PS_C-**4**	4.5e−1	1.7e−1	ND	4.2e−1	3.3e−1	1.9e0	2.1e−1	1.4e0	ND	ND	8.9e−1	1.9e0	ND	ND	1.9e0
S_PR_C-**4**	7.7e−1	6.3e−1	6.3e0	1.3e0	1.2e0	4.3e0	1.2e1	1.4e1	5.0e1	6.4e1	3.1e1	3.1e1	1.6e1	4.7e1	1.7e1
S_PS_C-**4**	1.6e−2	3.3e−1	2.1e0	ND	5.e-1	3.2e0	2.9e0	6.5e0	1.2e1	2.4e1	5.7e1	8.1e0	4.2e0	5.6e0	6.1e0
R_P-**5**	ND	3.8e1	5.9e0	2.5e1	2.2e1	1.7e1	8.1e−1	ND	9.7e−1	ND	ND	ND	2.2e0	ND	3.3e0
S_P-**5**	ND	ND	5.1e0	1.3e−1	4.1e−1	7.2e0	1.9e1	3.1e0	4.7e1	4.4e1	2.6e1	3.1e1	4.4e1	1.2e2	1.2e2

[a]The standard errors, from fits of the data to eq 1, are less than 20% of the stated values. ND, not determined.

Table 4. Values of k_{cat}/K_m (M^{-1} s^{-1}) for Wild-Type PTE and Its Mutants[a]

	WT	QF	YT	RN	QFRN	YTRN	GWT	GWT-d1	GWT-d2	GWT-d3	GWT-f1	GWT-f2	GWT-f3	GWT-f4	GWT-f5
R_P-**1**	4.9e5	1.5e6	2.4e3	1.7e5	3.0e6	4.3e3	1.5e3	2.5e3	6.1e3	9.1e3	1.0e5	5.2e4	6.1e3	7.2e3	8.5e3
S_P-**1**	1.2e6	7.1e6	1.6e5	7.4e5	8.0e6	1.7e5	2.2e5	1.9e5	1.2e6	1.2e6	7.2e5	6.2e5	1.3e5	2.3e5	2.9e5
R_P-**2**	5.8e5	8.2e5	2.5e3	2.8e5	1.6e6	3.4e3	1.8e3	3.5e3	6.0e3	8.1e3	1.4e4	4.7e3	3.4e3	4.2e3	6.1e3
S_P-**2**	2.7e4	1.2e6	1.1e5	2.6e4	1.6e6	1.4e5	5.9e4	8.6e4	4.6e5	4.3e5	1.4e5	1.9e5	1.2e5	2.4e5	4.2e5
R_P-**3**	8.5e5	3.1e5	1.3e4	4.0e5	1.3e6	1.3e4	1.5e3	3.0e3	5.4e3	7.6e3	3.3e3	3.8e3	8.2e2	2.6e3	2.2e3
S_P-**3**	3.4e4	1.6e6	7.3e4	4.8e4	1.4e6	3.9e5	1.8e5	5.0e5	1.1e6	1.2e6	6.7e5	1.0e6	1.1e6	2.3e6	1.9e6
R_PR_C-**4**	1.3e3	1.9e2	5.8e1	3.0e3	2.8e2	3.0e2	2.2e2	6.8e2	6.4e2	5.6e2	4.2e2	4.1e2	6.3e2	7.9e2	8.5e2
R_PS_C-**4**	2.0e2	5.5e1	1.6e1	4.6e2	7.4e1	1.9e2	1.3e2	1.2e2	1.5e2	1.4e2	2.1e2	1.4 e2	1.4e2	2.0e2	1.8e2
S_PR_C-**4**	1.1e2	1.6e3	1.8e3	2.3e2	1.8e3	1.2e3	8.1e3	2.3e4	6.0e4	8.7e4	1.3e4	1.4e4	3.2e3	5.0e3	3.8e3
S_PS_C-**4**	3.2e0	6.2e1	2.5e2	1.5e1	9.6e1	4.8e2	1.7e3	4.2e3	8.1e3	1.1e4	2.6e3	2.5e3	1.5e3	1.5e3	1.2e3
R_P-**5**	1.6e4	5.2e3	1.9e3	1.7e4	9.0e3	3.5e3	2.5e2	3.0e2	5.4e2	5.5e2	6.0e2	8.6e2	4.5e2	5.1e2	7.7e2
S_P-**5**	2.1e1	3.3e2	5.8e3	2.8e1	3.6e2	1.4e4	2.8e4	1.0e4	5.2e4	1.5e5	3.9e4	7.7e4	1.2e5	2.5e5	3.2e5

[a]The standard errors, from fits of the data to eq 1, are less than 20% of the stated values.

positioned between the side chains of the two histidine residues (Figure 5D).

Several changes in structure are observed in GWT-d3 without bound ligands compared to the structures of GWT-d3 complexed with compound **7** and GWT (PDB entries 1P6B and 1P6C, respectively). The indole ring of Trp-257 moves 1.2 Å closer to the glycine at position 254; the phenyl group of Phe-306 is 0.98 Å closer to the binuclear metal center, and Thr-303 is twisted with the side chain hydroxyl group pointing inward toward the binding pocket surface. However, there are no major differences in the active site residues in the GWT-d3 structure complexed with compound **7** and GWT.

The amino acid residues in the binding pocket of GWT-f5 with compounds **6** and **7** exhibit several alterations compared to the parental GWT structure (PDB entries 1P6B and 1P6C, respectively). The indole ring of Trp-257 moves 2.0 Å closer to the leucine at residue position 317 because more space is provided by the shorter leucine side chain than by methionine. The indole ring of Trp-131 is displaced around 1.0 Å, and the mutation of residue 132 shifts the main chain 1.1 Å (Figure 6A). In a comparison of the structures of GWT-f5 with compounds **6** and **7**, the side chains of the isoleucine at position 271 are twisted; C^{δ} and $C^{\gamma 2}$ of Ile-271 are displaced 1.5 and 3.0 Å, respectively. The large *O*-cyclohexyl group of compound **7** is pointed toward the enlarged small pocket, and the small methyl group is between the smaller large pocket and the leaving group pocket.

Screening and Kinetic Analysis of Wild-Type and Mutant Enzymes on GB, GD, and GF. For the purposes of initial screening, specific activities were determined with 3 mM substrate (Table 5). The YT mutant was very active with all three substrates, and the YT-RN mutant had higher activity than the wild type with GD. Therefore, kinetic constants were determined for these enzyme−substrate combinations (Table 6). The stereospecificity of variants was determined by following the fluoride released during the complete hydrolysis of GB or GF using the 0.5 mM racemic substrate. Substantial differences in the rates for the individual enantiomers result in biphasic curves (data not shown). The specificity of GWT toward GF is known from polarimetry experiments,[9] while the stereopreference of the remaining variants was determined by the ability of the variant to complement the slow phase in the GWT-catalyzed reaction (Table 5). YT has the same stereopreference as GWT for GF and has previously been shown to have the same preference as GWT for GD.[5] The stereopreference for the variants toward GB was determined by the ability to complement the slow phase in the YT-catalyzed reaction (Table 5).

DISCUSSION

Wild-type PTE catalyzes the hydrolysis of the insecticide paraoxon with kinetic constants that approach values of $\sim 10^4$ s^{-1} and $\sim 10^8$ M^{-1} s^{-1} for k_{cat} and k_{cat}/K_m, respectively.[21] However, the catalytic efficiency of the wild-type enzyme for the hydrolysis of organophosphorus nerve agents is significantly lower, and the enzyme prefers the less toxic R_P-enantiomers relative to the more toxic S_P-enantiomers.[5] The degree of stereoselectivity exhibited by the wild-type enzyme for chiral substrates is dependent to a significant extent on the size of the substituents attached to the central phosphorus core.[6] The QF

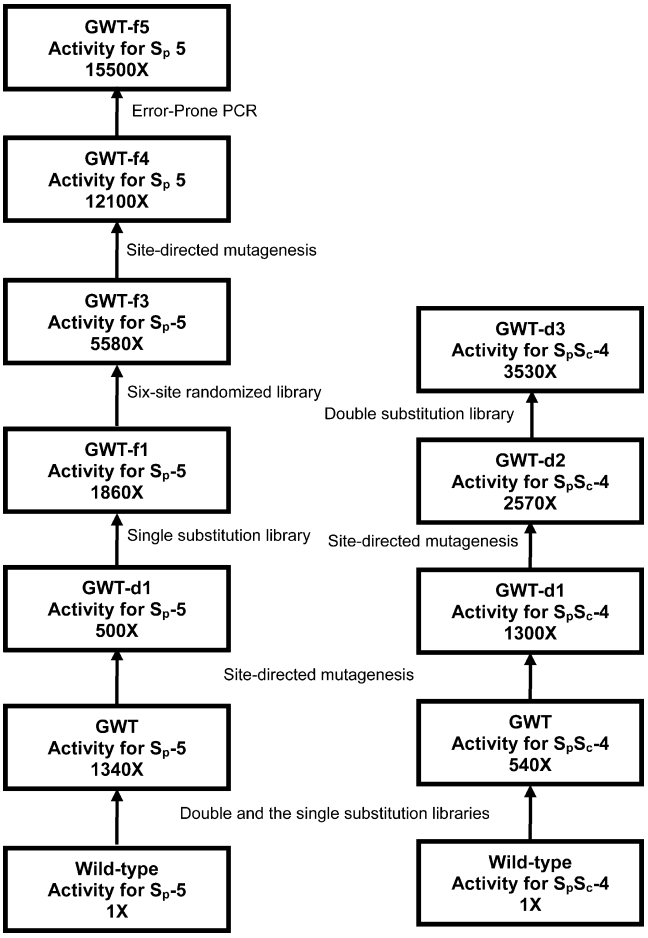

Figure 3. Outline of the parental lineage for the construction of mutants of PTE that are enhanced for the hydrolysis of S_P-**4** and S_P-**5**.

mutant was shown previously to exhibit the highest activity toward the more toxic S_P-enantiomers of compounds **1**−**3**, which are analogues of VX, GB, and VR, respectively.[5] The GWT mutant possessed the highest hydrolytic activity toward the more toxic S_P-enantiomers of compounds **4** and **5**, which are analogues of soman and cyclosarin, respectively.[5] These mutants were selected for further modification in an attempt to increase the catalytic activity of PTE through directed evolution.

The introduction of the K185R and I274N modifications into PTE was initiated in an attempt to increase net protein expression levels and solubility. These two mutations also enhanced the hydrolytic activity for some of the compounds presented in Scheme 2. The QF-RN mutant has higher values of k_{cat} and k_{cat}/K_m for most of the compounds tested, relative to those of the parent QF mutant. QF-RN has the best activity toward S_P-**1** and S_P-**2**, analogues of VX and sarin, respectively. Overall, the values of k_{cat}/K_m for these two compounds are 7- and 60-fold higher, respectively, than that of wild-type PTE, and the absolute magnitude of k_{cat}/K_m exceeds 10^6 M^{-1} s^{-1} for each compound.

An in vitro screening strategy was utilized to identify mutants that are further optimized starting from the GWT-d1 parent. The GWT-f1 enzyme contains an additional M317L mutation and is ∼4-fold better in terms of k_{cat}/K_m than the GWT-d1 mutant for the hydrolysis of S_P-**5** and ∼2000-fold better than wild-type PTE. The GWT-f1 mutant was subsequently

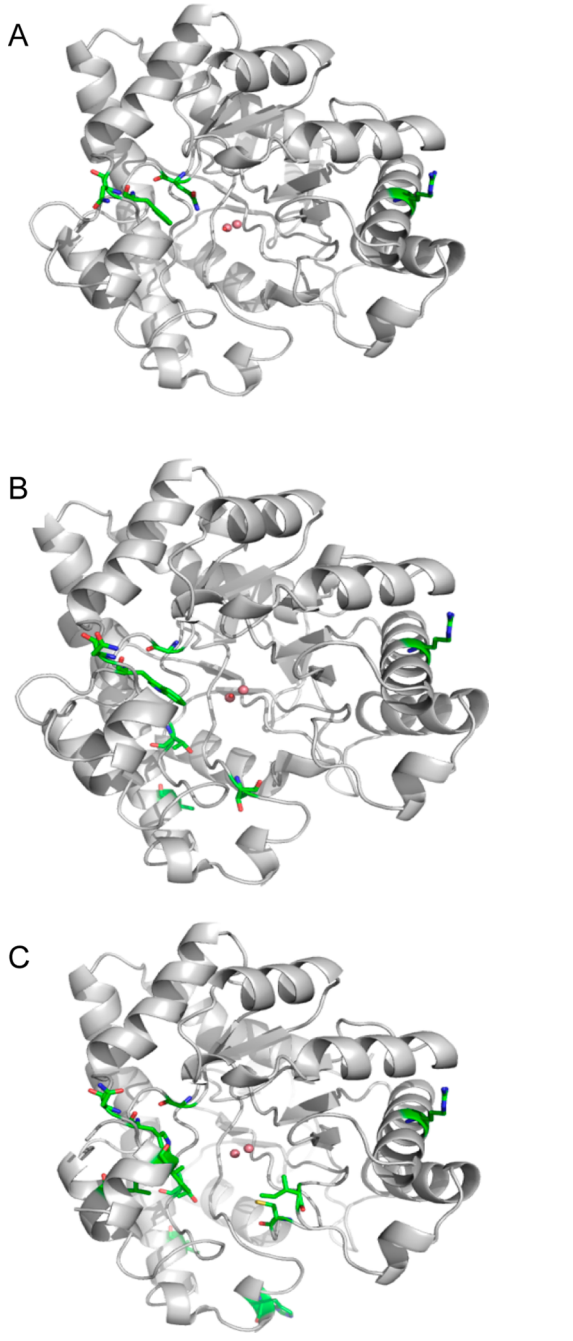

Figure 4. Localization of the mutations in QFRN (A), GWT-d3 (B), and GWT-f5 (C). The mutated residues are colored green.

coexpressed with GpdQ in *E. coli* cells. These cells can grow in a phosphate-free minimal medium with a 165 h lag phase using S_P-**5** as the sole phosphorus source. Therefore, the in vivo selection method is practical when S_P-**5** is used to screen large mutant libraries. GWT-f3 was identified from a mutant library containing six partially randomized residues within the active site of PTE. The additional changes to the protein sequence included I106C, F132I, and L271I. GWT-f3 was ∼3-fold better in terms of k_{cat}/K_m than the GWT-f1 parent and ∼6000-fold better than wild-type PTE for the hydrolysis of S_P-**5**.

The A80V mutation was added to GWT-f3 to create the GWT-f4 mutant. This change increased the catalytic efficiency for the hydrolysis of S_P-**5** ∼2-fold. The GWT-f4 mutant was subjected to error-prone PCR mutagenesis, and GWT-f5 with

dx.doi.org/10.1021/bi300811t | *Biochemistry* 2012, 51, 6463−6475

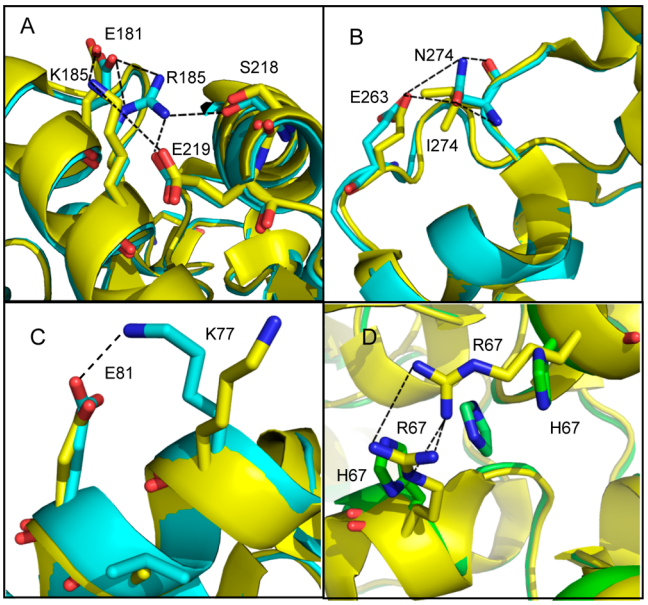

Figure 5. Structural perturbations at the mutated sites in GWT-d3 and GWT-f5. (A) The parent enzyme (GWT) in the region of Lys-185 is colored yellow and the mutant, GWT-d3, cyan. (B) The parent enzyme (GWT) in the region of I274 is colored yellow and the mutant, GWT-d3, cyan. (C) The parent enzyme (GWT) in the region of Ala-80 is colored yellow and the mutant, GWT-f5, cyan. (D) The parent enzyme (GWT) in the region of Arg-67 is colored yellow and the mutant, GWT-f5, green. An imidazole is found in a π-stacking arrangement between the two histidine residues at the subunit interface.

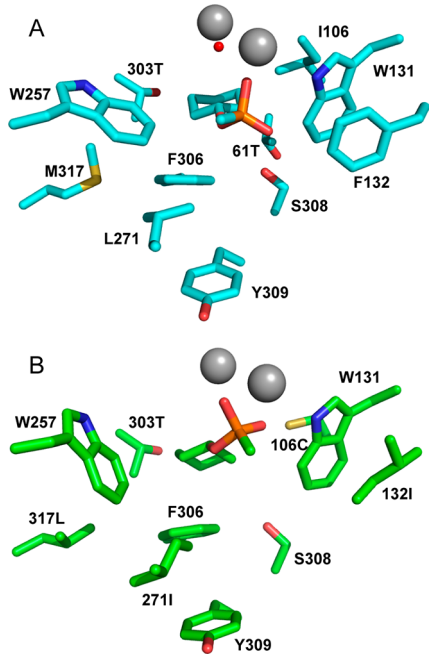

Figure 6. Substrate binding pocket of GWT-d3 (A) and GWT-f5 (B) complexed with compound 7.

an R67H substitution was identified using the selection strategy in phosphate-free medium with S_P-**5** as the sole phosphorus source. GWT-f5 was ~50% more active for the hydrolysis of S_P-**5** than the parent enzyme, and the value of k_{cat}/K_m was ~3 × 10^5 M^{-1} s^{-1}. This is the best mutant for the hydrolysis of the GF analogue, and it is ~15000-fold better than the wild-type enzyme. GWT-f5 is also the best mutant for the hydrolysis of S_P-**3**, the analogue of the nerve agent VR. For this compound, the value of k_{cat}/K_m is ~2 × 10^6 M^{-1} s^{-1} and the rate enhancement, relative to that of the wild-type enzyme, is increased by nearly 2 orders of magnitude.

We have previously shown that the GpdQ diesterase is unable to hydrolyze the product produced by the action of PTE on S_PS_C-**4** and S_PR_C-**4**, analogues of the two most toxic diastereomers of soman.[21,31] Therefore, the selection strategy for the identification of beneficial mutations for the hydrolysis of these compounds could not be utilized. Nevertheless, utilization of the in vitro screening approach yielded mutants with substantially enhanced kinetic constants. GWT was previously identified as being a good catalyst for the hydrolysis of the two S_P-diastereomers of compound **4**. The addition of the RN mutations to this variant gave GWT-d1. These changes enhanced the values of k_{cat}/K_m by a factor of ~3 for the hydrolysis of each compound relative to that of GWT. The addition of the A80V mutation to GWT-d1 further enhanced the hydrolysis rates an additional 2−3-fold. Finally, the GWT-d2 mutant was modified with two double-substitution libraries, and the S61T change was identified via screening of individual colonies. GWT-d3 is nominally better than GWT-d2 for the hydrolysis of the S_P-diastereomers of compound **4**. Overall, GWT-d2 is enhanced ~800-fold, relative to the wild-type enzyme, for the hydrolysis of S_PR_C-**4** and ~3500-fold for the hydrolysis of S_PS_C-**4**. The absolute values of k_{cat}/K_m for the hydrolysis for S_PR_C-**4** are ~10^5 and 10^4 M^{-1} s^{-1} for the hydrolysis of S_PS_C-**4**.

While analogues **1**−**5** contain the authentic chiral centers seen in the nerve agents, the leaving groups are very different,

Table 5. Activity of Wild-Type and Mutant Enzymes with Racemic G-Agents[a]

enzyme	GB	GD	GF	GB[b] preferred enantiomer	GF[b] preferred enantiomer
WT	303	14	363	NA[c]	R_P
YT	843	212	240	S_P	S_P
YT-RN	263	115	116	S_P	S_P
QF-RN	32	1.0	41	NA[c]	NA[c]
GWT	20	2.0	44	S_P	S_P
GWT-d1	57	2.0	7	S_P	S_P
GWT-d2	52	1.0	211	S_P	S_P
GWT-d3	48	8	35	S_P	S_P
GWT-f3	142	10	94	S_P	S_P
GWT-f5	240	19	59	S_P	S_P

[a]In micromoles per minute per milligram of protein. [b]Determined with 0.5 mM racemic substrate. [c]No significant stereopreference under these conditions.

Table 6. Kinetic Constants for Hydrolysis of GB, GD, and GF[a]

enzyme	substrate	k_{cat} (s^{-1})	K_m (μM)	k_{cat}/K_m (M^{-1} s^{-1})
WT	GB	430 ± 50	1800 ± 400	2.4 (0.6) × 10^5
WT	GD	12 ± 1	800 ± 200	1.5 (0.4) × 10^4
WT	GF	210 ± 30	900 ± 300	2.3 (0.8) × 10^5
YT	GB	520 ± 30	260 ± 50	2.0 (0.4) × 10^6
YT	GD	240 ± 20	460 ± 90	5 (1) × 10^5
YT	GF	130 ± 10	170 ± 50	8 (2) × 10^5
YTRN	GD	100 ± 10	300 ± 100	4 (2) × 10^5

[a]Racemic mixtures of GB, GD, and GF were used for these measurements.

dx.doi.org/10.1021/bi300811t | *Biochemistry* 2012, 51, 6463−6475

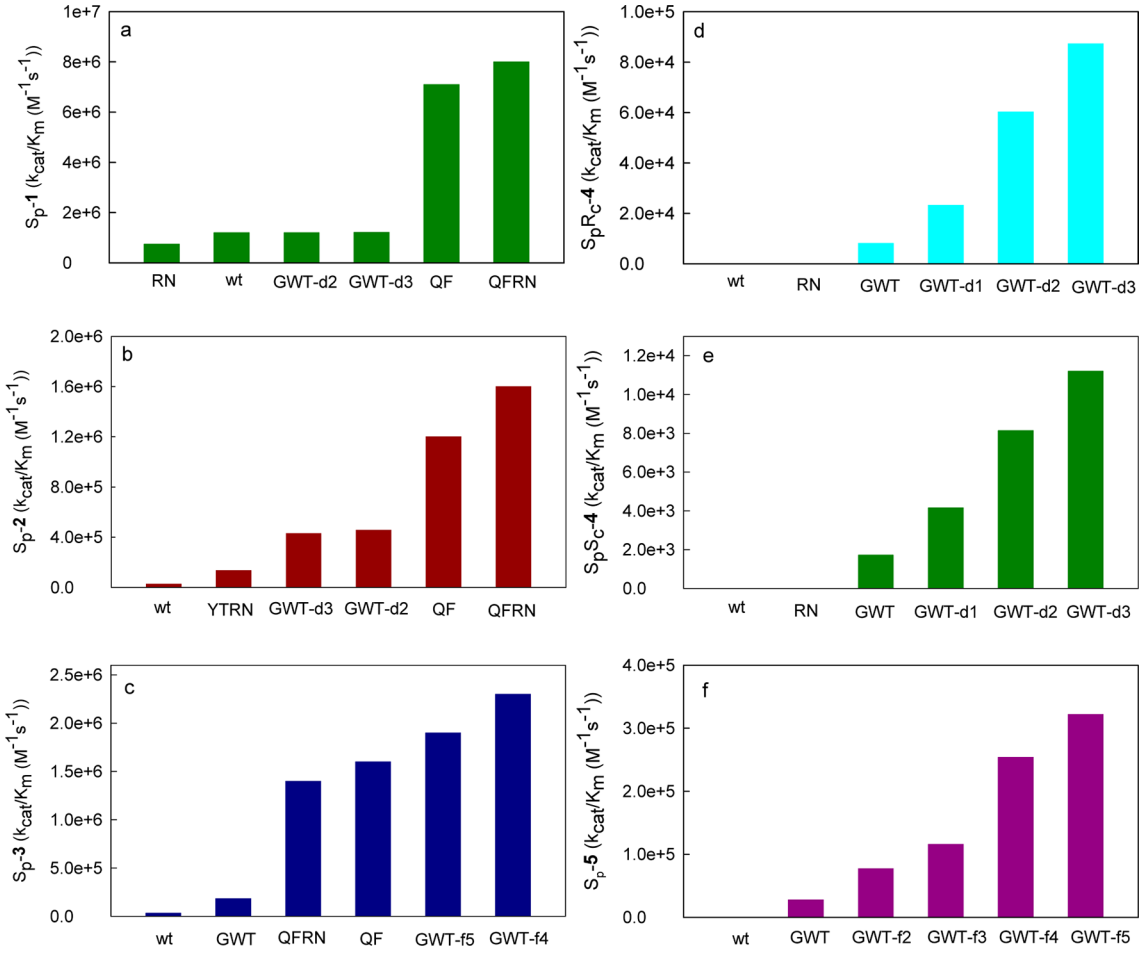

Figure 7. Bar graphs illustrating enhanced values for k_{cat}/K_m (M^{-1} s^{-1}) for the S_P-enantiomer of compounds **1** (a), **2** (b), **3** (c), S_PR_C-**4** (d), S_PS_C-**4** (e), and **5** (f) as catalyzed by the wild-type and engineered mutants of PTE.

making verification of the analogue data important. Variant GWT-d3 was developed with the GD analogue (**4**) and displays a 4-fold improvement over the GWT parent with authentic GD. This correlates well with the 6-fold improvement predicted by the analogue. It is important to note that the wild-type enzyme hydrolyzes the toxic S_PS_C-enantiomer of GD more than 15-fold slower than the other three enantiomers, while GWT hydrolyzes this enantiomer with a rate similar to that of the S_PR_C-enatiomer.[5] The measured rate of hydrolysis of racemic GD is relatively low, but the enhancements in the GWT-d3 variant, which has the same stereoselectivity profile as GWT, represent a >60-fold improvement against the toxic enantiomers of GD. Similarly, the variants that were developed for the hydrolysis of GF (GWT-f3 and GWT-f5) are specific for the hydrolysis of the S_P-enantiomer. Wild-type PTE is known to hydrolyze the S_P-enantiomer ~20-fold slower than the R_P-enantiomer, while the GWT variant prefers the S_P-enantiomer by 6-fold.[9] The absolute value of the measured activity against the racemic GF is lower for the improved variants, but when the switch in specificity is taken into account, the activity against the S_P-enantiomer of GF improved ~3-fold for GWT and GWT-f5 and ~5-fold for the GWT-f3 variant as predicted from the analogue studies.

The data collected with authentic nerve agents did contain some unexpected results. Variants GWT-f3 and GWT-f5 were substantially enhanced versus GWT for the hydrolysis of both GB and GD with a nearly 1 order of magnitude improvement seen for both nerve agents. Similarly, the GWT-d2 variant is 5-fold better than GWT against GF and, when the different stereopreference is taken into account, >1 order of magnitude better than the wild type for the hydrolysis of the S_P-enantiomer. The best variant identified to date against GB, GD, and GF is the YT variant with k_{cat}/K_m values of 2.0×10^6, 5×10^5, and 8×10^5 M^{-1} s^{-1}, respectively. Not only is this variant significantly improved over wild-type PTE for all of the nerve agents, it also prefers the more toxic S_P-enantiomers.

The other enzymes that are known to hydrolyze the G-type nerve agents, organophosphorus acid anhydrolase (OPAA), diisopropylfluorophosphatase (DFPase), and human paraoxonase 1 (hPON1), have catalytic efficiencies that lag behind that of the YT variant of PTE. The G-agents are hydrolyzed by OPAA with high k_{cat} values of ~600 s^{-1} (GB), 3100 s^{-1} (GD), and 1700 s^{-1} (GF), but the K_m values for all of the G-agents are estimated to be between 1 and 10 mM; it is known that OPAA is selective for the less toxic R_P-enantiomers of the G-agents.[32−34] The YT mutant of PTE has an ~1 order of magnitude better catalytic efficiency against GB. Similarly, the high K_m values of OPAA for GD and GF and the known preference for the hydrolysis of the R_P-enantiomers make the activity of the YT variant active substantially better against the more toxic S_P-enantiomers.

Variants optimized for the S_P-enantiomers of the G-agents have been reported for both DFPase and hPON1. The improved hPON1 variant shows little stereoselectivity against

dx.doi.org/10.1021/bi300811t | *Biochemistry* 2012, 51, 6463−6475

GB, but the reported k_{cat}/K_m value of 5×10^3 M^{-1} s^{-1} is significantly below that of the YT variant.[35] The best DFPase variant is selective for the S_P-enantiomer of GB and has a k_{cat}/K_m value of 2.3×10^5 M^{-1} s^{-1}, but the K_m is greater than 10 mM.[36] The optimized DFPase variants prefer the S_P-enantiomers of GD and GF, but the K_m values are in excess of 10 mM. For GF, the best variant of DFPase has a k_{cat}/K_m value of 2.3×10^5 M^{-1} s^{-1}, which is somewhat below that measured for the YT variant.[36] The optimized hPON1 variant has k_{cat}/K_m values for the two S_P-enantiomers of GD of 1.2×10^5 and 1×10^4 M^{-1} s^{-1}, both of which are below the values measured for the YT variant of PTE, and the k_{cat}/K_m value for S_P-GF of 2.9×10^5 M^{-1} s^{-1} is ~2.5-fold lower than that of the YT variant.[35]

The X-ray crystal structures of QF-RN, GWT-d3, and GWT-f5 show that the K185R and I274N mutations provide additional hydrogen bonding interactions with adjacent amino acid resides. Molecular modeling of the RN mutations predicted that Glu-219 and Glu-181 could form hydrogen bonds with the newly introduced Arg-185 and that Glu-263 could potentially form a hydrogen bond with the newly introduced Asn-274 residue.[28] The crystal structures of QF-RN, GWT-d3, and GWT-f5 demonstrated that Ser-218 can also form hydrogen bond with Arg-185. These crystal structures demonstrate that the K185R and I274N mutations provide more hydrogen bonding interactions with neighboring amino acid residues that could enhance the conformational stability. In the GWT-d3 and GWT-f5 structures with compound **7**, the large cyclohexyl group of compound **7** points toward the enlarged small pocket. This suggests that the more toxic S_P-diastereomers of compounds **1**−**5** may enter active site of PTE with the larger substituents of these compounds pointing toward the enlarged small pocket and preferentially hydrolyzed with higher activities.

Given the dramatic changes in activity, it is somewhat surprising that no major structural changes to the active site are observed in the improved variants. The majority of changes to active site residues involve the movement of side chains by only 1−2 Å. The slight changes to the protein scaffold caused by the new hydrogen bonding networks and alterations to the active site combine to bring about dramatic changes in the activity and stereoselectivity. The diminutive nature of these changes makes them hard to predict, but the strategy outlined in Figure 3 has allowed significantly improved variants to be identified. This combination of site-directed mutagenesis, active site library screening, and in vivo selection has allowed the development of variants with altered stereoselectivity and rate enhancements for hydrolysis of compounds **1**−**5**. GWT from the first generation of mutants was demonstrated to have an inverted stereoselectivity and enhanced catalytic activity toward the more toxic S_P-enantiomers of the soman and cyclosarin analogues.[5] The structural modifications to GWT within the substrate binding pocket, surface, and dimer interface have substantially enhanced substrate binding and catalytic turnover. The changes in the k_{cat}/K_m values of the S_P-enantiomers of the organophosphonates are illustrated in Figure 7.

■ ASSOCIATED CONTENT

Accession Codes

The X-ray coordinates and structure factors for the PTE mutants have been deposited in the Protein Data Bank: 3UR2, 3UPM, 3URA, 3URN, 3URB, 3URQ and 3UR5.

■ AUTHOR INFORMATION

Corresponding Author

*F.M.R.: telephone, (979) 845-3373; fax, (979) 845-9452; e-mail, raushel@tamu.edu. D.P.B.: telephone, (979) 458-0735; fax, (979) 845-4719; e-mail, barondeau@chem.tamu.eu.

Funding

This work was supported in part by the NIH (GM 68550).

Notes

The authors declare no competing financial interest.

■ ABBREVIATIONS

PTE, phosphotriesterase; GpdQ, glycerophosphodiesterase; OpdA, organophosphate degrading enzyme from *A. radiobacter*; PEG MME, polyethylene glycol monomethyl ether; rmsd, root-mean-square deviation.

■ REFERENCES

(1) Dumas, D. P., Durst, H. D., Landis, W. G., Raushel, F. M., and Wild, J. R. (1990) Inactivation of organophosphorus nerve agents by the phosphotriesterase from *Pseudomonas diminuta*. *Arch. Biochem. Biophys. 277*, 155−159.

(2) Lai, K., Grimsley, J. K., Kuhlmann, B. D., Scapozza, L., Harvey, S. P., DeFrank, J. J., Kolakowski, J. E., and Wild, J. R. (1996) Rational enzyme design: Computer modeling and site-directed mutagenesis for the modification of catalytic specificity in organophosphorus hydrolase. *Chimia 50*, 430−431.

(3) Raveh, L., Segall, Y., Leader, H., Rothschild, N., Levanon, D., Henis, Y., and Ashani, Y. (1992) Protection against tabun toxicity in mice by prophylaxis with an enzyme hydrolyzing organophosphate esters. *Biochem. Pharmacol. 22*, 397−400.

(4) Caldwell, S. R., Newcomb, J. R., Schlecht, K. A., and Raushel, F. M. (1991) Limits of diffusion in the hydrolysis of substrates by the phosphotriesterase from *Pseudomonas diminuta*. *Biochemistry 30*, 7438−7444.

(5) Tsai, P. C., Bigley, A., Li, Y., Ghanem, E., Cadieux, C. L., Kasten, S. A., Reeves, T. E., Cerasoli, D. M., and Raushel, F. M. (2010) Stereoselective hydrolysis of organophosphate nerve agents by the bacterial phosphotriesterase. *Biochemistry 49*, 7978−7987.

(6) Chen-Goodspeed, M., Sogorb, M. A., Wu, F., Hong, S. B., and Raushel, F. M. (2001) Structural determinants of the substrate and stereochemical specificity of phosphotriesterase. *Biochemistry 40*, 1325−1331.

(7) Chen-Goodspeed, M., Sogorb, M. A., Wu, F., and Raushel, F. M. (2001) Enhancement, relaxation, and reversal of the stereoselectivity for phosphotriesterase by rational evolution of active site residues. *Biochemistry 40*, 1332−1339.

(8) Nowlan, C., Li, Y., Hermann, J. C., Evans, T., Carpenter, J., Ghanem, E., Shoichet, B. K., and Raushel, F. M. (2006) Resolution of chiral phosphate, phosphonate, and phosphinate esters by an enantioselective enzyme library. *J. Am. Chem. Soc. 128*, 15892−15902.

(9) Harvey, S. P., Kolakowski, J. E., Chen, T. C., Rastogi, V. K., Reiff, L. P., DeFrank, J. J., Raushel, F. M., and Hill, C. (2005) Stereospecificity in the enzymatic hydrolysis of cyclosarin (GF). *Enzyme Microb. Technol. 37*, 547−555.

(10) Benschop, H. P., and Dejong, L. P. A. (1988) Nerve Agent Stereoisomers: Analysis, Isolation, and Toxicology. *Acc. Chem. Res. 21*, 368−374.

(11) Hill, C. M., Li, W. S., Thoden, J. B., Holden, H. M., and Raushel, F. M. (2003) Enhanced degradation of chemical warfare agents through molecular engineering of the phosphotriesterase active site. *J. Am. Chem. Soc. 125*, 8990−8991.

(12) Li, W. S., Lum, K. T., Chen-Goodspeed, M., Sogorb, M. A., and Raushel, F. M. (2001) Stereoselective detoxification of chiral sarin and soman analogues by phosphotriesterase. *Bioorg. Med. Chem. 9*, 2083−2091.

(13) Cho, C. M.-H., Mulchandani, A., and Chen, W. (2006) Functional analysis of organophosphorus hydrolase variants with high degradation activity towards organophosphate pesticides. *Protein Eng., Des. Sel. 19*, 99−105.
(14) Cho, C. M.-H., Mulchandani, A., and Chen, W. (2004) Altering the substrate specificity of organophosphorus hydrolase for enhanced hydrolysis of chlorpyrifos. *Appl. Environ. Microbiol. 70*, 4681−4685.
(15) Roodveldt, C., and Tawfik, D. S. (2005) Directed evolution of phosphotriesterase from *Pseudomonas diminuta* for heterologous expression in *Escherichia coli* results in stabilization of the metal-free state. *Protein Eng., Des. Sel. 18*, 51−58.
(16) Yang, H., Carr, P. D., McLoughlin, S. Y., Liu, J. W., Horne, I., Qiu, X., Jeffries, C. M., Russell, R. J., Oakeshott, J. G., and Ollis, D. L. (2003) Evolution of an organophosphate-degrading enzyme: A comparison of natural and directed evolution. *Protein Eng. 16*, 135−145.
(17) Reetz, M. T., Carballeira, J. D., and Vogel, A. (2006) Iterative saturation mutagenesis on the basis of B factors as a strategy for increasing protein thermostability. *Angew. Chem., Int. Ed. 45*, 7745−7751.
(18) Machius, M., Declerck, N., Huber, R., and Wiegand, G. (2003) Kinetic stabilization of *Bacillus licheniformis* α-amylase through introduction of hydrophobic residues at the surface. *J. Biol. Chem. 278*, 11546−11553.
(19) Ghanem, E., Li, Y., Xu, C., and Raushel, F. M. (2007) Characterization of a phosphodiesterase capable of hydrolyzing EA 2192, the most toxic degradation product of the nerve agent VX. *Biochemistry 46*, 9032−9040.
(20) McLoughlin, S. Y., Jackson, C., Liu, J. W., and Ollis, D. L. (2004) Growth of *Escherichia coli* coexpressing phosphotriesterase and glycerophosphodiester phosphodiesterase, using paraoxon as the sole phosphorus source. *Appl. Environ. Microbiol. 70*, 404−412.
(21) Aubert, S. D., Li, Y., and Raushel, F. M. (2004) Mechanism for the hydrolysis of organophosphates by the bacterial phosphotriesterase. *Biochemistry 43*, 5707−5715.
(22) Otwinowski, Z., and Minor, W. (1997) Processing of X-ray diffraction data collected in oscillation mode. *Methods Enzymol. 276*, 307−326.
(23) McCoy, A. J., Grosse-Kunstleve, R. W., Adams, P. D., Winn, M. D., Storoni, L. C., and Read, R. J. (2007) Phaser crystallographic software. *J. Appl. Crystallogr. 40*, 658−674.
(24) Murshudov, G. N., Vagin, A. A., and Dodson, E. J. (1997) Refinement of macromolecular structures by the maximum-likelihood method. *Acta Crystallogr. D53*, 240−255.
(25) Collaborative Computational Project, Number 4 (1994) The CCP4 suite: Programs for protein crystallography. *Acta Crystallogr. D50*, 760−763.
(26) McRee, D. E. (1999) XtalView/Xfit: A Versatile Program for Manipulating Atomic Coordinates and Electron Density. *J. Struct. Biol. 125*, 156−165.
(27) Brunger, A. T., Adams, P. D., Clore, G. M., DeLano, W. L., Gros, P., Grosse-Kunstleve, R. W., Jiang, J.-S., Kuszewski, J., Nilges, N., Pannu, N. S., Read, R. J., Rice, L. M., Simonson, T., and Warren, G. L. (1998) Crystallographic and NMR system (CNS): A new software system for macromolecular structure determination. *Acta Crystallogr. D54*, 905−921.
(28) Bruns, C. M., Hubatsch, I., Ridderstrom, M., Mannervik, B., and Tainer, J. A. (1999) Human glutathione transferase A4-4 crystal structures and mutagenesis reveal the basis of high catalytic efficiency with toxic lipid peroxidation products. *J. Mol. Biol. 288*, 427−439.
(29) Wanner, B. L. (1994) Molecular genetics of carbon-phosphorus bond cleavage in bacteria. *Biodegradation 5*, 175−184.
(30) Kononova, S. V., and Nesmeyanova, M. A. (2002) Phosphonates and their degradation by microorganisms. *Biochemistry (Moscow, Russ. Fed.) 67*, 184−195.
(31) Benschop, H. P., Konings, C. A. G., Genderen, J. V., and DeJong, L. P. A. (1984) Isolation, anticholinesterase properties, and acute toxicity in mice of the four stereoisomers of the nerve agent soman. *Toxicol. Appl. Pharmacol. 72*, 61−74.
(32) DeFrank, J. J., Beaudry, W. T., Cheng, T.-C., Harvey, S. P., Stroup, A. N., and Szafraniec, L. L. (1993) Screening of halophilic bacteria and *Alteromonas* species for organophosphorus hydrolyzing enzyme activity. *Chem.-Biol. Interact. 87*, 141−148.
(33) Cheng, T.-C., Liu, L., Wang, B., Wu, J., DeFrank, J. J., Anderson, D. M., Rastogi, V. K., and Hamilton, A. B. (1997) Nucleotide sequence of a gene encoding an organophosphorus nerve agent degrading enzyme from *Alteromonas haloplanktis*. *J. Ind. Microbiol. Technol. 18*, 49−55.
(34) Hill, C. M., Li, W.-S., Cheng, T.-C., DeFrank, J. J., and Raushel, F. M. (2001) Stereochemical specificity of organophosphorus acid anhydrolase toward *p*-nitrophenyl analogs of soman and sarin. *Bioorg. Chem. 29*, 27−35.
(35) Gupta, R. D., Goldsmith, M., Ashani, Y., Simo, Y., Mullokandov, G., Bar, H., Ben-David, M., Leader, H., Margalit, R., Silman, I., Sussman, J. L., and Tawfik, D. S. (2011) Directed evolution of hydrolases for prevention of G-type nerve agent intoxication. *Nat. Chem. Biol. 7*, 120−125.
(36) Melzer, M., Chen, J. C.-H., Heidenreich, A., Gab, J., Koller, M., Kehe, K., and Blum, M. M. (2009) Reversed enantioselectivity of diisopropyl fluorophosphatase against organophosphorus nerve agents by rational design. *J. Am. Chem. Soc. 131*, 17226−17232.